Chapter 5
A Hybrid Control Approach to Nanopositioning

Tomas Tuma, Abu Sebastian, John Lygeros, and Angeliki Pantazi

Abstract Precise position control on the nanometer and subnanometer scale, referred to as nanopositioning, is a key enabler for nanoscale science and engineering. In nanopositioning, feedback control is essential to meet the stringent requirements on accuracy, stability, and repeatability in the presence of model uncertainties and environmental disturbances. In this chapter, we review a new hybrid control approach to nanopositioning which is based on the combination of a continuous-time control law with impulsive modifications of the controller states. By using impulsive control, the limitations of conventional linear controllers can be overcome, such as the inherent trade-off between closed-loop bandwidth and resolution. We review the related literature, present an in-depth analysis of the stability and performance characteristics of impulsive control, and verify the theoretical conclusions experimentally using a custom-built atomic force microscope.

5.1 Introduction

The burgeoning field of nanoscale science and nanotechnology was arguably started in the 1980s with the invention of the scanning tunneling microscope [1] and the atomic force microscope (AFM) [2], two instruments which form the foundation of scanning probe microscopy (SPM), allowing us to interact with matter on scales down to the size of a single atom. Scanning probe techniques are currently

T. Tuma • A. Sebastian (✉) • A. Pantazi
IBM Research - Zurich, 8803 Rüschlikon, Switzerland
e-mail: uma@zurich.ibm.com; ase@zurich.ibm.com; agp@zurich.ibm.com

J. Lygeros • T. Tuma
ETH Zurich, 8092 Zürich, Switzerland
e-mail: lygeros@control.ee.ethz.ch

M. Rakotondrabe (ed.), *Smart Materials-Based Actuators at the Micro/Nano-Scale: Characterization, Control, and Applications*, DOI 10.1007/978-1-4614-6684-0_5,

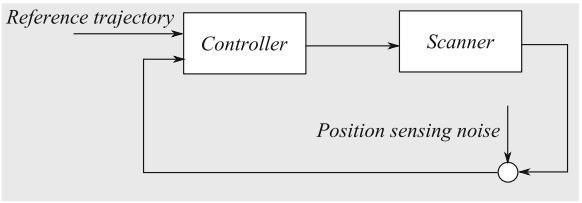

Fig. 5.1 A schematic of a feedback control loop as often encountered in nanopositioning. The controller forces the scanner to follow the desired reference trajectory by generating an actuation signal according to a control law based on the reference trajectory and a feedback measurement signal of the scanner position. The measurements are typically affected by sensing noise

used in the exploration of molecular structure [3], fabrication of nanometer-scale objects [4], observation of biological phenomena in real time [5], high-density data storage [6, 7], and characterization of semiconductor devices [8].

In SPM, precise control of motion with a subnanometer accuracy is of key importance. Nanometer-scale objects and their properties, such as topographical, electrical, and magnetic properties, are examined by means of a microfabricated cantilever with an atomically sharp tip at its end. Typically, the tip of the cantilever is positioned with subnanometer accuracy relative to the sample by means of a nanopositioner, and the sample properties are inferred from the forces acting on the tip. For example, to resolve the topography of a surface, the cantilever tip can be moved in a raster-based pattern across a rectangular scan area, and a three-dimensional estimate of the topography is obtained from analyzing the deflection of the tip. The accuracy of the nanopositioner, or scanner, is vital for the overall performance of the microscope.

In achieving the stringent accuracy requirements in nanopositioning, the concept of feedback control plays a pivotal role. Feedback controllers are essential in compensating for exogenous disturbances, such as building vibrations, temperature fluctuations, and manufacturing imperfections. Moreover, actuation techniques with ultra-high resolution, such as those using piezoelectric actuators, often exhibit significant nonlinearities (e.g., hysteresis, creep, and drift) which need to be compensated for by means of control. If high-speed operation is required, the complex dynamical behavior of the scanner also needs to be taken into account to prevent unwanted scanner-induced vibrations.

Figure 5.1 shows a schematic of a feedback loop as often encountered in nanopositioning. Here, the scanner is controlled by means of a feedback and/or feedforward controller whose inputs are the reference trajectory and the measurement signal. Based on the reference and the measurement signals, the controller executes a control law and makes the scanner follow the desired reference trajectory. The measurement signal is affected by additive measurement noise.

This chapter reviews a novel hybrid control approach to nanopositioning in which the controller combines a continuous-time control law with a discrete control law based on impulsive changes of the controller state. By using this impulsive state multiplication (ISM), some principal limitations of linear control can be overcome,

such as the trade-off between the closed-loop bandwidth and the positioning resolution. Moreover, impulsive control is an important theoretical concept which links hybrid control with some of the recent nonlinear control techniques for nanopositioning and enables new and elegant ways to analyze and improve them. Despite its nonlinear character, impulsive control is easy to implement and can significantly improve the performance of existing nanopositioning systems. The exposition in this chapter is based on the theoretical and experimental results published in [9–12].

First, we briefly review the landscape of feedback control for nanopositioning in Sect. 5.2. Section 5.3 introduces the concept of impulsive control and its particular type, ISM, and analyzes the stability of linear systems with impulses. Section 5.4 presents control architectures based on impulsive feedback control, including feedback controllers for tracking piecewise constant and piecewise affine reference signals, and analyzes their performance. Section 5.5 discusses an inherent connection between impulsive control and the recently published signal transformation approach (STA) to nanopositioning, including techniques to significantly improve the transient performance of STA. Section 5.6 contains extensive experimental results, which demonstrate the properties of impulsive control and STA in a custom-built high-speed AFM. Section 5.7 concludes the chapter.

5.2 Feedback Control for Nanopositioning

In the design of feedback controllers for nanopositioning, specific control challenges must be taken into account, such as the high amount of measurement noise and the complex dynamical behavior of nanopositioners. In what follows, we review some of the recent linear and nonlinear control approaches in nanopositioning. The review includes an extensive account on the existing linear and nonlinear feedback control techniques in nanopositioning, which provides the necessary context for introducing the concept of impulsive control in Sect. 5.3.

5.2.1 Linear Feedback Control

Linear feedback controllers have been widely used in nanopositioning because of their conceptual and implementational simplicity [13–15]. Conventional linear feedback controllers are often based on the proportional, integral, and derivative (PID) control components. However, PID control often cannot meet the increasing requirements on robustness, accuracy, and speed. For instance, PI controllers inherently impose a trade-off between robustness and performance which becomes prohibitive in complex high-speed nanopositioning devices, especially when high bandwidth is of critical importance. Hence, a significant research effort has been devoted to developing advanced linear feedback architectures for nanopositioning and design methodologies.

Resonant control [16–18] is another technique which is used in nanopositioning as an alternative to conventional PI controllers. In integral resonant control, the controller consists of a constant feed-through term and a first-order integral feedback controller. Resonant controllers are well suited for damping of vibrations in systems with collocated actuators and sensors and are robust and simple to implement.

Advanced linear control techniques can improve the performance and design trade-offs of feedback control for nanopositioning, but they are subject to inherent constraints [19,20]. For example, there is a fixed mathematical relationship between the closed-loop sensitivity and complementary sensitivity transfer functions which dictates a trade-off between the tracking bandwidth and the positioning resolution [21]. At the same time, constraints such as Bode's integral law limit the shape of the closed-loop sensitivity transfer function. Consequently, bandwidth, positioning resolution, and robustness requirements often pose a significant challenge in linear feedback control.

In two-degree-of-freedom (2DOF) control [22], the control laws which act on the reference and measurement signals are specified independently. This is in contrast to the conventional single degree of freedom controller, which typically operates on the difference between the reference and the measurement signal. By using 2DOF controllers, the transfer functions among the reference signal, measurement noise, and output can be designed independently, which allows better design trade-offs.

5.2.2 Feedback Control of Repetitive Reference Signals

In many nanopositioning control problems, the reference signals are determined by the physics of the underlying application and can be exploited in the control design. In particular, the reference signals in SPM are often repetitive. For example, in raster scanning SPM, the tip is positioned relative to the sample along consecutive scan lines, which typically requires repetitive reference signals such as triangular or saw waveforms.

Repetitive reference signals can be tracked with tailored feedback controllers. In adaptive control [23], the control law itself is adapted online to improve the tracking performance. In repetitive control [24, 25], the feedback loop is augmented with a signal generator which recreates the *a priori* known reference signal, typically by means of a pure delay element. By doing so, the repetitive tracking error can be reduced after a certain number of iterations at the price of increased settling time, implementation complexity, and robustness issues. Iterative learning control (ILC) [26] is a similar learning-based concept in which, in contrast to repetitive control, the initial conditions are reset at every iteration and hence, discontinuous operation is possible. ILC-based controllers can achieve nearly perfect tracking but might result in a significant computation complexity which imposes requirements on the digital signal-processing hardware.

5.2.3 Feedforward Control and Reference Signal Shaping

Feedback control is often combined with feedforward control in which the dynamics and nonlinear characteristics of the actuator, such as creep and hysteresis, are anticipated, modeled, and inverted [27]. Feedforward control can significantly improve the closed-loop performance. However, it depends on the availability of accurate models and can be severely affected by changes in the plant dynamics. In some cases, nonlinear characteristics can be suppressed or inverted by using special hardware, such as in the case of charge-driven piezoelectric actuators. This simplifies the control design but increases the complexity and cost of the hardware.

A special case of feedforward control is command pre-shaping, i.e. shaping or modifying of the reference signal. For instance, vibrations induced by the reference signal can be reduced by using impulse input sequences [28]. In raster scanning SPM, shaping of the turnaround points of triangular waveforms has been extensively used and matured into a useful technique [29]. Most recently, alternative SPM scan trajectories which result in dramatically different reference signals have been proposed, such as spiral [30–32], cycloid [33], and Lissajous [34] scan trajectories. These trajectories can also be obtained by mathematical optimization [35].

5.2.4 Hybrid Feedback Control

Hybrid systems are dynamical systems that combine continuous and discrete dynamics [36]. They arise naturally in sampled digital control architectures and in applications where dynamical systems are combined with discrete logic. For example, in the framework of switched systems [37], multiple linear feedback controllers are switched depending on various algebraic and logical conditions, such as the operating points of the plant. Hybrid control systems are a particularly promising technique for advanced control of mechanical systems: on the one hand, like nonlinear systems, they have the potential of overcoming the fundamental limitations of linear feedback control; on the other hand, they allow the use of well-established linear control techniques in combination with nonlinear control laws.

One of the earliest developments of this kind in the field of applied hybrid control is the Clegg integrator [38]. Clegg observed that in a feedback loop with a single integrator, the phase lag due to the integral component can be significantly decreased if the state of the integrator is reset to zero whenever its input reaches zero. Denoting the integrator state $x(t)$ and its input $e(t)$, the dynamics of a Clegg integrator in state-space are

$$\dot{x}(t) = e(t) \text{ when } e(t) \neq 0 \tag{5.1}$$

$$x(t) := 0 \text{ for } e(t) = 0 \tag{5.2}$$

For instance, if $e(t)$ is the tracking error, resetting the integrator state when the tracking error is zero reduces the unnecessary overshoot caused by $x(t) \neq 0$ when the error is already removed. The effect of the reset control law is quite significant: the magnitude response of the integral controller remains unchanged, the phase lag decreases from 90° to only about 50°.

More generally, the Clegg integrator belongs to the class of reset control systems which have been further generalized and studied both theoretically and experimentally [39–41]. The concept of reset control is conceptually close to that of impulsive control, which will be studied in the remainder of this chapter.

5.3 Impulsive Control

Dynamical systems which evolve continuously but are subject to sudden impulses or impacts arise naturally and are one of the basic hybrid phenomena. Examples include colliding particles, bouncing balls, and systems with mechanical impacts. In a general treatment, impulsive systems have been studied thoroughly [42]. This chapter reviews a control concept recently introduced in nanopositioning and based on impulsive changes of the states of a linear feedback controller. We shall introduce a particular type of impulsive control namely, ISM, and analyze the stability and performance of the resulting hybrid impulsive system.

5.3.1 Impulsive State Multiplication

In ISM, the state of a dynamical system is multiplied by given factors at discrete time instants.

Let $\{t_i\}_{i=1}^{\infty}$ denote a sequence of time instants such that $0 = t_1 < t_2 < \cdots < t_i < \cdots$. Let $\{Q_i\}_{i=1}^{\infty}$ be a sequence of real square multiplication matrices $Q_i \in \mathbb{R}^{n\times n}$ for $i = 1, 2, \ldots$. The multiplication matrices will be referred to as state multiplication matrices (SMM), and in what follows, they will be assumed to be diagonal

$$Q_i = \begin{bmatrix} q_{i1} & 0 & \ldots & 0 \\ 0 & q_{i2} & \ldots & 0 \\ \ldots & & & \\ 0 & \ldots & & q_{in} \end{bmatrix} \tag{5.3}$$

for $i = 1, 2, \ldots$; n is the number of states in the state vector.

Definition 1. Let K be a linear, time-invariant system with state space matrices (A, B, C, D). *K with ISM* is a dynamical system that evolves according to the following equations:

$$\dot{x}(t) = Ax(t) + Bu(t) \text{ when } t \neq t_i, i = 1,2,3,\ldots \tag{5.4}$$

$$x(t_i) := Q_i x(t_i^-) \text{ for } i = 1,2,3,\ldots \tag{5.5}$$

$$y(t) = Cx(t) + Du(t) \tag{5.6}$$

where $t \in \mathbb{R}_+$, $x_K(t) \in \mathbb{R}^n$, $u(t) \in \mathbb{R}^m$, $y(t) \in \mathbb{R}^p$, $A \in \mathbb{R}^{n\times n}$, $B \in \mathbb{R}^{n\times m}$, $C \in \mathbb{R}^{p\times n}$, $D \in \mathbb{R}^{1\times m}$ and will be denoted as

$$\text{ISM}(K, \{t_i\}_{i=1}^{\infty}, \{Q_i\}_{i=1}^{\infty}). \tag{5.7}$$

The assumption on the diagonality of SMM is not critical; however, it simplifies the analysis because it excludes any state coupling at the time of the multiplication.

5.3.2 Stability

Linear systems with ISM are subject to instantaneous state changes at predefined time instants. Because a stable linear system can be destabilized with ISM, the stability of the resulting hybrid system must be studied carefully with respect to the impulse magnitudes and timing. In the following, we present a bounded-input-bounded-output stability theorem for ISM-based systems.

Theorem 1. *Consider a system with ISM*

$$\text{ISM}(K, \{t_i\}_{i=1}^{\infty}, \{Q_i\}_{i=1}^{\infty})$$

Assume that

$$0 < t_{i+1} - t_i < \Theta$$

and that the input signal is bounded, i.e.

$$\|u(t)\|_\infty < \infty$$

If there exists $q < 1$ *such that*

$$\left\|e^{A(t_{i+1}-t_i)}Q_i\right\| < q$$

for $i = 1,2,3\ldots$ *then*

$$\|x(t)\|_\infty < \infty$$

The proof of Theorem 1 is relatively straightforward and can be found in [9]. The theorem parallels the results known from the theory of impulsive systems as elaborated, e.g., in [42]. While the theorem guarantees bounded-input-bounded-state stability when only an upper bound on the time between impulses is assumed, stronger results can be obtained, e.g., when the average time between the impulses is

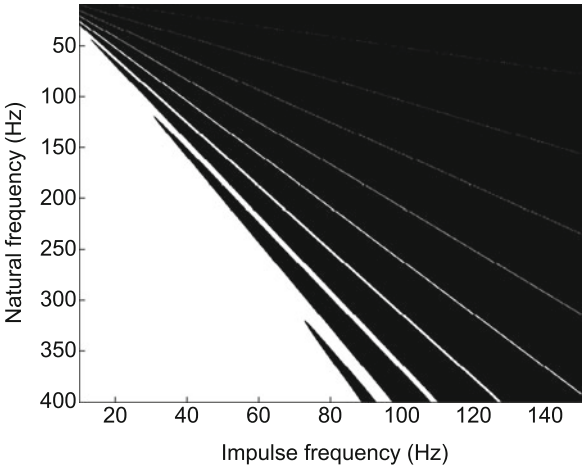

Fig. 5.2 Sufficient condition for stability of a second-order system under regular impulses. The *plots* show the quantity $\|e^{AT}Q_i\|$ as a function of the frequency of the impulses applied and the natural frequency and the damping coefficient of the plant, respectively. *White* corresponds to values smaller than one, *black* corresponds to values greater than or equal to one. The system is guaranteed to be stable in the *white* parameter region. Figure ©IEEE 2012, reprinted from [9] with permission

considered. This approach is well known in switched systems [37]. Theorem 1 sheds light onto the relation between the frequency and the magnitude of the impulses and the dynamics of the linear system required for stability. For example, if the time between the impulses is fixed, $T := t_{i+1} - t_i$ for $i \in \mathbb{N}$, and the magnitude of the impulses is upper bounded by Q such that $\|Q_i\| \leq Q$ for $i \in \mathbb{N}$, the stability condition can be rewritten as

$$\|e^{AT}\| < 1/Q. \tag{5.8}$$

Hence, if the stability condition applies, the possible locations of the system poles are limited. It can be shown that an upper bound on the real part of the system poles is

$$\Re(\lambda) \leq \frac{1}{T} \log \|e^{AT}\| < -\frac{\log Q}{T}. \tag{5.9}$$

For $Q > 1$, i.e., when the impulses magnify some of the states, $\log Q > 0$ and the real parts of the poles are enforced to be less than a negative number i.e. proportional to the frequency of the impulses. When $Q \leq 1$, the upper bound shifts to nonnegative numbers, suggesting that poles with a nonnegative real part may be present in a stable impulsive system. Indeed, such systems can be found, for instance, by constantly counteracting a state growth with an appropriate impulsive control law.

In the following, we demonstrate the stability condition for a second-order system with natural frequency ω_n and damping coefficient $\xi = 0.3$. Figure 5.2

shows the stability criterion as a function of the impulse frequency $1/T$ and the plant parameter ω_n. The impulse magnitude is uniform and fixed as $Q_i = \begin{bmatrix} 2 & 0 \\ 0 & 2 \end{bmatrix}$. The white region depicts the parameter space in which stability is guaranteed, the dark region depicts the parameter space in which $\|e^{AT} Q_i\| > 1$ and stability is not guaranteed. It is apparent that a high damping coefficient and/or a high natural frequency are vital for stability; stability is not guaranteed if fast impulses are applied to plants which are relatively "slow" or insufficiently damped. It also becomes clear that the frequency of the impulses may interfere with the natural frequency of the plant. For instance, the line-shaped stability regions in Fig. 5.2 arise when the impulses align with the natural frequency ω_n, e.g., when $T = c/\omega_n$ for some $c \in \mathbb{N}$. In such a case, the stability may be guaranteed even for very high impulse frequencies.

5.4 Impulsive Control for Feedback Systems

In this section, the concept of ISM is applied to feedback control. A novel control architecture is presented in which a linear feedback controller is extended into a hybrid system with ISM.

The control architecture is based on a one degree of freedom, single-input-single-output feedback loop which combines linear and impulsive control as shown in Fig. 5.3. The aim of the controller, K, is to force the plant, P, to track the reference signal, r. The controller consists of a linear feedback and a linear feedforward component, K_{FB} and K_{FF}, respectively. The feedback component is subject to impulsive state changes by the ISM block which can be driven either by the reference or by the measurement signals. The control and measurement signals are affected by the input disturbance signal, d_{i}, the output disturbance signal, d_{o}, and the measurement noise, n.

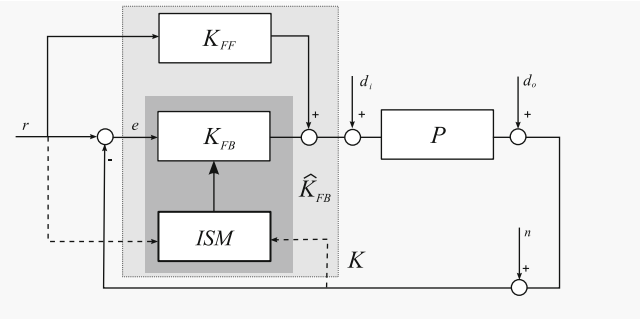

Fig. 5.3 Control architecture combining linear and impulsive control. Plant P is controlled by controller K comprising a feedforward component, K_{FF}, and a feedback component, K_{FB}. The *ISM* block impulsively modifies the states of K_{FB} based on the reference or measurement signals. Figure ©IEEE 2012, reprinted from [9] with permission

In what follows, we present a control design for tracking piecewise constant and piecewise affine reference signals that is based on the control architecture shown in Fig. 5.3. Piecewise constant and piecewise affine reference signals are widely used in nanopositioning and specially in SPM. The control architectures we present can significantly improve the tracking bandwidth for these reference signals without increasing the sensitivity to measurement noise. Thereby, they overcome one of the fundamental limitations of linear feedback systems. Finally, a general methodology is presented for the design of more complex control architectures, such as those for feedback control with multiple control objectives.

5.4.1 Tracking of Piecewise Constant Signals

In the following, a linear feedback control loop with a single integrator for tracking of piecewise constant signal is extended with ISM-based control laws.

Definition 2. A piecewise constant signal $r(t)$, $t \geq 0$ is determined by a series of time instants $\{t_i\}_{i=1}^{\infty}$ and values $\{v_i\}_{i=0}^{\infty}$ such that $r(t) = v_i$ when $t \in [t_{i-1}, t_i)$ for $i \in \mathbb{N}$.

First, consider the control scheme of Fig. 5.3 with $ISM = 0$, $K_{\mathrm{FF}} = 0$, and P with no poles at the origin and assume that the controller involves a single integrator. In such a control scheme, a step signal can be tracked with a zero steady-state error. Because a piecewise constant signal can be viewed as a series of steps, it can also be tracked if the control loop has a sufficient bandwidth. The tracking will result in a short transient effect at the points of step changes and near-zero tracking error elsewhere.

By using impulsive control, the tracking performance of the single integral controller $K_{\mathrm{FB}} = k/s$ can be improved without increasing the controller bandwidth. This can be done by using the state multiplication matrix (SMM).

$$Q_i = \left[\frac{v_i}{v_{i-1}} \right] \tag{5.10}$$

for $i \in \mathbb{N}$, which multiplies the state of the feedback controller at time instants t_i, $i \in \mathbb{N}$, by the ratio of the successive reference signal values. It can be shown that by using this SMM, the tracking error decays exponentially for any piecewise constant signal if the plant dynamics can be neglected:

Theorem 2. *Consider the control scheme in Fig. 5.3 with* $K_{\mathrm{FF}} = 0$, $K_{\mathrm{FB}} = \frac{k}{s}$. *If* $P(s) = 1$, *all disturbance signals are zero and* $r(t) = v_i$ *for* $t \in [t_{i-1}, t_i)$, $i \in \mathbb{N}$, *the controller*

$$\hat{K}_{\mathrm{FB}} = \mathrm{ISM}\left(\frac{k}{s}, \{t_i\}_{i=1}^{\infty}, \left\{ \left[\frac{v_i}{v_{i-1}} \right] \right\}_{i=0}^{\infty} \right)$$

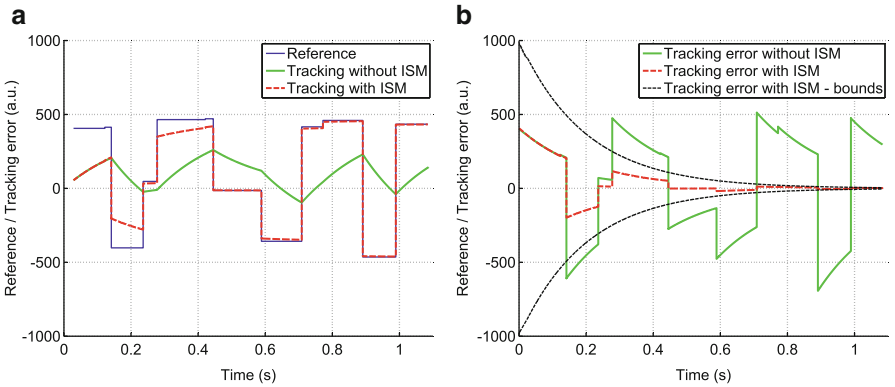

Fig. 5.4 Tracking of a piecewise constant reference signal with and without impulsive control (ISM). With impulsive control, the tracking error converges to zero despite the low bandwidth of the controller. The controller bandwidth governs the error bounds (shown in (**b**)), which decay exponentially to zero. (**a**) System output. (**b**) Tracking error. Figure ©IEEE 2012, reprinted from [9] with permission

tracks the reference signal with error

$$e(t) = v_i e^{-kt}.$$

Theorem 2 bounds the tracking error of an impulsive system with a single integral controller and a piecewise constant reference on an ideal plant. It says that the reference is tracked with an error that decays exponentially to zero.

We illustrate the results of Theorem 2 through simulations. A piecewise constant reference signal (shown in Fig. 5.4a as thin blue curve) was randomly generated and tracked on an ideal plant, $P(s) = 1$, with a single integral feedback controller $K(s) = 5/s$. The bandwidth of the controller is less than 1 Hz, which is very low compared with the bandwidth of the reference signal. Consequently, the reference signal is tracked poorly and with a large tracking error, as shown in Fig. 5.4a and Fig. 5.4b by the thick green curve. When K is equipped with ISM, the resulting feedback controller $\hat{K}$ is the nonlinear system

$$\hat{K} = \mathrm{ISM}\left(\frac{5}{s}, \{t_i\}_{i=1}^{\infty}, \left\{\left[\frac{v_i}{v_{i-1}}\right]\right\}_{i=0}^{\infty}\right). \tag{5.11}$$

In controller $\hat{K}$, the impulsive control law multiplies the state of the low bandwidth integrator by the ratio of the successive values of the reference signal. By doing so, a near-perfect tracking performance is achieved after a short transition period (shown in Fig. 5.4a, b as dashed red curve). The duration of the transition period and the magnitude of the tracking error can be derived from Theorem 2. The bounds on the tracking error (up to the scaling by v_i) are indicated in Fig. 5.4b by the solid black curve.

The assumption of $P(s) = 1$ is critical for the validity of Theorem 2 and translates into the requirement of a sufficient bandwidth and damping of the plant in the frequency region where impulses are applied. In many practical scenarios, this requirement is fulfilled: nanopositioners are often designed specifically for high bandwidth [43] and their dynamics may in addition be improved by active or passive damping [44, 45]. Also, the linearity of the nanopositioner is important. For nanopositioners based on intrinsically nonlinear actuators, such as piezoelectric tube actuators or piezo-stack actuated flexure stages, a linearizing stage has to precede the application of impulsive control. Alternatively, in the case of piezoelectric actuation, using a charge amplifier instead of the conventional voltage amplifier to drive them can bring about sufficient linearity [46].

5.4.2 *Tracking of Piecewise Affine Signals*

Similar to piecewise constant signals, piecewise affine signals can be tracked by extending a linear feedback loop with an ISM-based control law.

Definition 3. A piecewise affine signal $r(t)$, $t \geq 0$, is determined by a series of time instants $\{t_i\}_{i=1}^{\infty}$, offsets $\{v_i\}_{i=0}^{\infty}$ and slopes $\{w_i\}_{i=0}^{\infty}$ such that

$$r(t) = v_i + w_i(t - t_{i-1}) \tag{5.12}$$

when $t \in [t_{i-1}, t_i)$ for $i \in \mathbb{N}$.

Definition 3 defines a piecewise affine signal as a sequence of ramp-like signals with successive segments that do not necessarily share their endpoints. In addition, we will assume that the ramp always has a nonzero slope, i.e., $w_i \neq 0$ for $i \in \mathbb{N}$. The class of piecewise affine signals includes some of the signals widely used in nanopositioning, such as triangular waveforms with constant or varying speed and amplitude.

In the control framework of Fig. 5.3, piecewise affine reference signals can be tracked using a feedforward gain compensation and a single integral feedback controller. If the plant, P, has a nonzero, finite DC gain k_P which is known exactly, feedforward compensation with a constant term is applicable, i.e. $K_{\mathrm{FF}} = \frac{1}{k_P}$. With this feedforward compensation, it can be shown that a single integral feedback controller $K_{\mathrm{FB}}(s) = \frac{k}{s}$ tracks a ramp reference signal with a zero steady-state error. Consequently, given sufficient bandwidth of the system, also a piecewise affine reference can be tracked.

By employing impulsive control, fast piecewise affine signals can be tracked even with low bandwidth K_{FB}. The ISM control law that can do this originates from the control architecture for piecewise constant signals derived in Sect. 5.4.1; the problems are linked because tracking piecewise affine signals inherently involves tracking piecewise constant signals. This can be shown for various families of

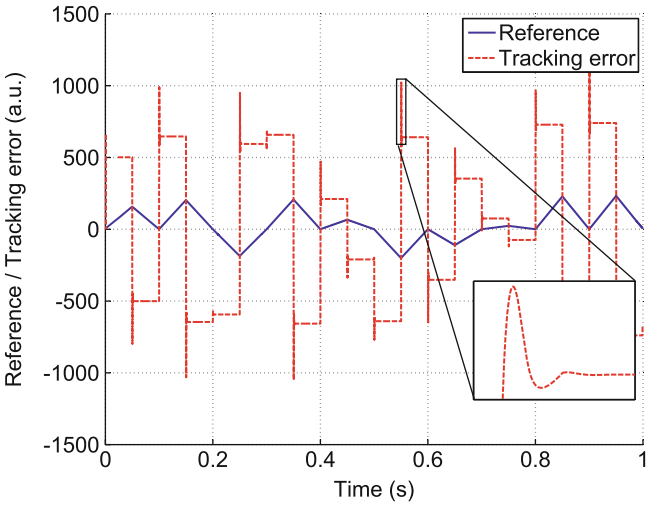

Fig. 5.5 Tracking of a piecewise affine signal on a second-order positioner (simulation). The tracking error is approximately piecewise constant and is determined by the slope of the reference signal. Figure ©IEEE 2012, reprinted from [9] with permission

plants, e.g., for linear, time-invariant plants with a nonzero, finite gain and proper transfer function [9]. For these plants, the steady-state tracking error under a ramp input is constant and proportional to the slope of the ramp. If the bandwidth of the plant is sufficiently high, such that the transients can be neglected, the tracking error can be approximated by a constant. Hence, because a piecewise affine signal is just a sequence of ramp signals, the tracking error for a piecewise affine reference signal is approximately a piecewise constant signal, provided the bandwidth of the plant is sufficiently high. Therefore, the tracking error can be reduced by applying the techniques presented in Sect. 5.4.1.

Figure 5.5 illustrates these observations in simulation for a second-order plant with natural frequency 1 kHz and damping ratio 0.5. A random triangular waveform with different amplitudes and slopes was applied to the plant and the output was subtracted from the input to obtain the tracking error. The tracking error is approximately piecewise constant, with short transients at the points where the reference signal changes the slope. The character of the transients depends on the bandwidth and damping of the plant.

Having realized that the tracking error can be approximated by a piecewise constant signal whose values are proportional to the slope of the ramp, w_i, and applying the results presented in Sect. 5.4.1, the SMM for tracking piecewise affine signals becomes

$$Q_i = \left[\frac{w_i}{w_{i-1}}\right] \tag{5.13}$$

for $i \in \mathbb{N}$. This SMM multiplies the state of the feedback controller by the ratio of the successive slopes of the reference signal. By doing so, the tracking error for piecewise affine signals can be reduced under the same conditions as discussed in Sect. 5.4.1, namely, for sufficiently damped plants the tracking error diminishes according to the exponential bounds of Theorem 2.

5.4.3 Feedback Control with Multiple Control Objectives

In the control architecture of Fig. 5.3, the ISM component is able to simultaneously execute multiple impulsive control laws which are based on different input signals and affect different states of the linear controller. Such a configuration is needed when more complex or multiple control objectives have to be met. A general way to design an ISM-based feedback control architecture in such a case is to partition the states of the linear controller and apply different ISM control laws to different parts of the controller.

Consider that the feedback controller, K_{FB}, is decomposed as

$$K_{\mathrm{FB}}(s) = \sum_{j=1}^{N} K_{\mathrm{FB}}^{j}(s), \tag{5.14}$$

where K_{FB}^{j}, $j = 1,\ldots,N$ are the controller components. Assume that the realization of the i-th transfer function is $(A_{\mathrm{FB}}^{i}, B_{\mathrm{FB}}^{i}, C_{\mathrm{FB}}^{i})$ and consider the realization of the sum of transfer functions with

$$A_{\mathrm{FB}} = \begin{bmatrix} A_{\mathrm{FB}}^{1} & 0 & \ldots & & \\ 0 & A_{\mathrm{FB}}^{2} & 0 & \ldots & \\ \ldots & & & & \\ 0 & \ldots & 0 & A_{\mathrm{FB}}^{j} & 0 \ \ldots \\ \ldots & & & & \\ & & & & A_{\mathrm{FB}}^{N} \end{bmatrix}$$

and the state partitioned as

$$x_{\mathrm{FB}} = \begin{pmatrix} x_{\mathrm{FB}}^{1} & \ldots & x_{\mathrm{FB}}^{N} \end{pmatrix}$$

where $x_{\mathrm{FB}}^{j} \in \mathbb{R}^{n(j)}$, $j = 1,\ldots,N$, is the state of K_{FB}^{j} with the dimension $n(j) \in \mathbb{N}$. Accordingly, the input matrix

$$B_{\mathrm{FB}} = \begin{bmatrix} B_{\mathrm{FB}}^{1} & B_{\mathrm{FB}}^{2} \ldots & B_{\mathrm{FB}}^{N} \end{bmatrix}^{T} \tag{5.15}$$

where $B_{\mathrm{FB}}^j \in \mathbb{R}^{n(j)\times 1}$ is the input matrix of K_{FB}^j. The outputs of the controller components are added,

$$C_{\mathrm{FB}} = \left[C_{\mathrm{FB}}^1 \; C_{\mathrm{FB}}^2 \ldots C_{\mathrm{FB}}^N \right], \tag{5.16}$$

where $C_{\mathrm{FB}}^j \in \mathbb{R}^{1\times n(j)}$ is the output matrix of K_{FB}^j.

Assume that ISM is applied to the partitioned feedback controller,

$$\hat{K}_{\mathrm{FB}} := \mathrm{ISM}(K_{\mathrm{FB}}, \{t_i\}_{i=1}^{\infty}, \{Q_i\}_{i=1}^{\infty}). \tag{5.17}$$

The resulting impulsive controller, $\hat{K}_{\mathrm{FB}}$, has dynamics that evolve between the impulses, $t \neq t_i$, according to

$$\begin{aligned} \dot{\hat{x}}_K(t) &= A_{\mathrm{FB}}\hat{x}_K(t) + B_{\mathrm{FB}}e(t) \\ y(t) &= C_{\mathrm{FB}}\hat{x}_K(t), \end{aligned}$$

where $\hat{x}_K$ denotes the state of K and $e(t)$, $y(t)$ denote the system input and output, respectively. At the time of impulses, $t = t_i$, the state of K is multiplied

$$\hat{x}_K(t_i) := Q_i\hat{x}_K(t_i^-).$$

As the state $\hat{x}_K$ is partitioned according to the decomposition of the feedback controller, it is straightforward to partition the SMM:

$$Q_i = \begin{bmatrix} Q_i^1 & 0 & \ldots & & \\ 0 & Q_i^2 & 0 & \ldots & \\ \ldots & & & & \\ 0 & \ldots & 0 & Q_i^j & 0 \; \ldots \\ \ldots & & & & \\ & & & & Q_i^N \end{bmatrix}$$

In the partitioned SMM, $Q_i^j \in \mathbb{R}^{n(j)\times n(j)}$ is the SMM corresponding to the controller component K_{FB}^j. The advantage of the partitioning is that distinct impulsive control laws can be applied to the controller components. In the special case when Q_i^j is an identity matrix of appropriate dimensions, the corresponding states evolve linearly. When $Q_i^j = 0$, the corresponding states are reset to zero.

The method described above is general and can be applied to a wide variety of problems. The control architectures for tracking piecewise constant and piecewise affine signals presented above are one example thereof. In [9], an example in which multiple control objectives must be met simultaneously is elaborated. Experimental results using an ISM-based feedback loop to track a high-bandwidth reference signal in presence of significant input disturbance are presented in Sect. 5.6.

5.5 Relation Between Impulsive Control and Signal Transformation Approach

Recently, a new nonlinear control scheme for nanopositioning has been reported called STA [47]. STA is based on transformation of the reference, measurement, and control signals in a feedback loop. For example, triangular reference signals are tracked in STA by transforming the triangular waveforms into a ramp signal and vice versa. Interestingly, there is an inherent connection between STA and impulsive control which is analyzed in this section. The analysis has some important implications in the theoretical understanding of STA and leads to significant improvements in the implementation and performance of STA.

5.5.1 Signal Transformation Approach

STA is a control technique in which a linear feedback system is equipped with a pair of possibly time-invariant, nonlinear transformation functions. Consider the control scheme in Fig. 5.6. The transformation functions Φ, Φ^{-1} are mutually inverse and translate the signals between a low-bandwidth and high-bandwidth representation. Before the high speed reference signal enters the feedback loop, it is transformed by Φ into the low-bandwidth representation seen by the linear feedback controller K. The control effort that K generates is translated by Φ^{-1} before it is applied to the positioner to ensure that the desired reference signal is tracked. The measured output of the positioner is transformed by Φ back into the low-bandwidth representation.

The key idea of STA is that if the low-bandwidth representation of r is tracked accurately by K, the positioner follows the desired reference signal even if the bandwidth of K is much lower than what would be needed to track r in a conventional control architecture. The control framework of STA is general; specific transformation functions can be designed for the reference signals of interest.

One particular case is a triangular reference signal, which can be transformed into a ramp signal and vice versa by means of an affine, time-variant transformation [48, 49] as follows. Assume that the reference signal, $r(t)$, has frequency $f = 1/T$ and range $[0,A]$. For $t \geq 0$, divide the time into intervals corresponding to the half periods of the triangular waveform, $[(i-1)\frac{T}{2}, i\frac{T}{2})$ for $i \in \mathbb{N}$. In the odd

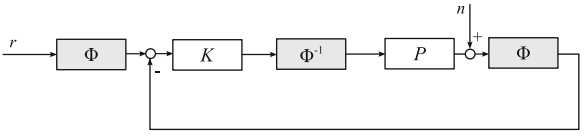

Fig. 5.6 Signal transformation approach to nanopositioning. A pair of mutually inverse transformation functions Φ, Φ^{-1} are used to transform the signals between a low-bandwidth and high-bandwidth representation. Figure ©Elsevier 2012, reprinted from [11] with permission

and even time intervals, $r(t)$ is strictly increasing and decreasing, respectively, and is governed by the equation

$$r(t) = (-1)^{(i-1)} \frac{2A}{T} \left(t - \lfloor \frac{i}{2} \rfloor T \right) \tag{5.18}$$

for $t \in [(i-1)\frac{T}{2}, i\frac{T}{2})$, $i \in \mathbb{N}$.

Definition 4. The forward and the inverse signal transformation operator, for conversion between a triangular waveform of frequency $1/T$ and range $[0,A]$ and a ramp signal with slope $2A/T$ are

$$\Phi(x(t),t) = (-1)^{(i-1)} x(t) + 2A \lfloor \frac{i}{2} \rfloor \tag{5.19}$$

for $t \in [(i-1)\frac{T}{2}, i\frac{T}{2})$, $i \in \mathbb{N}$.

$$\Phi^{-1}(x(t),t) = (-1)^{(i-1)} x(t) + (-1)^{i} 2A \lfloor \frac{i}{2} \rfloor \tag{5.20}$$

for $t \in [(i-1)\frac{T}{2}, i\frac{T}{2})$, $i \in \mathbb{N}$.

In the STA control scheme of Fig. 5.6, the above transformation functions can be used to facilitate the tracking of fast triangular waveforms by means of a low bandwidth double integral controller K. This is particularly beneficial in nanopositioning, wherein a low bandwidth K can be used for a control design with low sensitivity to the measurement noise, n.

5.5.2 ISM and Multiplicative Signal Transformation

The link between ISM and STA is based on the fact that multiplicative impulsive changes to the state of a linear system are equivalent to multiplicative transformation of the system input and output. This important fact is stated precisely in the following.

Consider the control scheme in Fig. 5.7. The input and output of a linear, time-invariant system K, are transformed by a pair of signal transformation operators J^{-1} and J, respectively. Assume that the time, $t \geq 0$, is divided into intervals $[t_{i-1}, t_i)$, $i \in \mathbb{N}$. The transformation operators are piecewise constant over the time intervals and multiply the signals as

$$\begin{aligned} J(u(t),t) &:= j_i u(t) \\ J^{-1}(u(t),t) &:= j_i^{-1} u(t) \end{aligned} \tag{5.21}$$

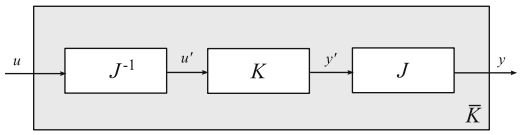

Fig. 5.7 Multiplicative signal transformation. The input and output of linear system K are transformed by a pair of mutually inverse multiplicative transformation operators. This scheme is equivalent to ISM applied to system K, thereby creating a link between ISM and STA. Figure ©Elsevier 2012, reprinted from [11] with permission

for $t \in [t_{i-1}, t_i)$, $i \in \mathbb{N}$. The multiplication factors j_i, $i \in \mathbb{N}$, are nonzero real numbers. At any given time point $t \in [t_{i-1}, t_i)$, the input signal, $u(t)$ is transformed into $u'(t) := j_i^{-1} u(t)$ and enters K. The output of K, $y'(t)$, is transformed as $y(t) = j_i y'(t)$. Hence, the input and output signals entering K are pre-multiplied and post-multiplied, respectively, by mutually inverse scalar factors.

The multiplicative signal transformation shown in Fig. 5.7 is tightly related to ISM. In fact, the following theorem holds:

Theorem 3. *For a given input $u(t)$, multiplication factors $\{j_i\}_{i=1}^{\infty}$ and times $\{t_i\}_{i=1}^{\infty}$, the output $y(t)$ of system $\bar{K}$ is the same as the output, $z(t)$, of the impulsive system*

$$\hat{K} := \mathrm{ISM}\left(K, \{t_i\}_{i=1}^{\infty}, \{\frac{j_{i+1}}{j_i} I\}_{i=1}^{\infty}\right) \tag{5.22}$$

for all times $t \geq 0$.

In other words, multiplicative signal transformation by factors j_i and $1/j_i$ is equivalent to ISM with SMM $Q_i = \frac{j_{i+1}}{j_i} I$. This fact can be shown by induction; the proof can be found in [11].

5.5.3 Tracking of Triangular Waveforms

Based on the relation between multiplicative impulsive changes to the state of a linear system and multiplicative signal transformation of its input and output presented in the preceding section, STA and ISM for tracking of triangular waveforms can be rigorously linked.

To reveal the connection between ISM and STA, the STA control scheme for tracking triangular waveforms (see Sect. 5.5.1) can be decomposed and simplified in a series of steps. This provides useful insights into the inherent properties of the scheme and reveals its relation to impulsive control. A detailed exposition is presented in [11]; in what follows, only the basic results are presented.

First, define the signal transformation operator

$$J(x(t), t) := (-1)^{i-1} x(t) \tag{5.23}$$

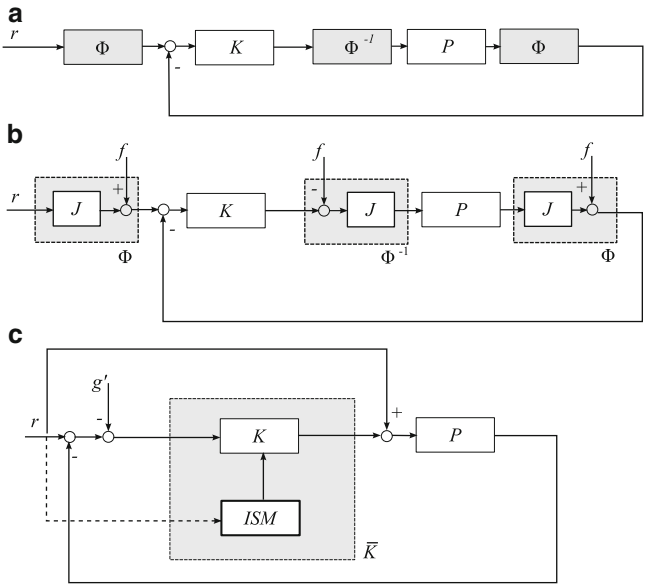

Fig. 5.8 Tracking of triangular waveforms: the relation between STA and ISM. (a) shows an STA control scheme with signal transformation blocks Φ and Φ^{-1}. (b) shows a control scheme equivalent to that shown in (a) with the signal transformation blocks decomposed. (c) shows an equivalent ISM-based control scheme

for $t \in [(i-1)\frac{T}{2}, i\frac{T}{2})$, $i \in \mathbb{N}$ where $1/T$ is the frequency of the triangular reference signal. The operator J inverts the sign of the input signal in the even half periods of the reference signal, i.e., when the triangular waveform is decreasing. It preserves the sign of the input signal in the odd half periods. Hence, J is the basic element of the transformation between a triangular waveform and a ramp signal.

Using the transformation operator J and defining an auxiliary stair-like signal $f(t)$, we realize that the signal transformation operators defined in Definition 4 can be expressed as

$$\Phi(x(t),t) = J(x(t),t) + f(t) \tag{5.24}$$

$$\Phi^{-1}(x(t),t) = J(x(t) - f(t),t) \tag{5.25}$$

Therefore, the control scheme of Fig. 5.8a is equivalent to the control scheme of Fig. 5.8b, with the transformation blocks decomposed.

By applying basic algebraic rules for signal flow diagrams and Theorem 3, the control scheme of Fig. 5.8b can be transformed into the control scheme shown in Fig. 5.8c, where the disturbance signal

$$g'(t) = (-1)^{i-1} \frac{2A}{k_1 T} e^{-\frac{k_2}{k_1} t} \tag{5.26}$$

for $t \in [(i-1)\frac{T}{2}, i\frac{T}{2})$, $i \in \mathbb{N}$, and the feedback controller is an ISM-based impulsive system

$$\mathrm{ISM}(K, \{i\frac{T}{2}\}_{i=1}^{\infty}, \{-I\}_{i=1}^{\infty}) \tag{5.27}$$

while yielding the same input–output relation.

The analysis reveals an important fact: the STA scheme for tracking triangular waveforms is equivalent to a negative feedback control loop with a constant-term feedforward connection and an impulsive feedback controller. The sign of the controller state is reversed at each turnaround point of the triangular reference signal. Furthermore, the analysis reveals the presence of a fixed bounded signal, $g'(t)$, which enters the feedback loop externally. The signal is implicit in the definition of the transformation operators and decays exponentially to zero; however, it is responsible for the large transient tracking error typically observed in the STA control loop.

5.5.4 Transient Performance of STA

The analysis presented in the preceding sections shows that the transient tracking error of STA for tracking triangular waveforms is strongly affected by the disturbance signal $g'(t)$ entering the feedback loop, see Fig. 5.8c. The disturbance signal is intrinsically generated by the signal transformation operators and depends on the reference signal, $r(t)$, and the double-integral feedback controller, K:

$$K(s) = \frac{k_1 s + k_2}{s^2} \tag{5.28}$$

Exact knowledge of the disturbance signal allows us to estimate the tracking error of STA analytically. It can be shown [11] that the tracking error induced by $g'(t)$ corresponds to a natural response of a second-order system with "damping coefficient" k_1 and "spring coefficient" k_2, with k_1 and k_2 being the integral gains of the feedback controller K. For example, if $k_2 > k_1^2/4$, the equation of the tracking error induced by the intrinsic disturbance signal is

$$|e_{g'}(t)| = \frac{2A/T}{\sqrt{k_2 - \frac{k_1^2}{4}}} e^{-\frac{k_1}{2}t} \sin t \sqrt{k_2 - \frac{k_1^2}{4}} \tag{5.29}$$

The equation says that the magnitude of the tracking error induced by $g'(t)$ is a sinusoidal waveform that exponentially decays to zero. It also shows that it is possible to design the feedback controller so that the transient response is "critically damped" by choosing gains k_1, k_2 that preserve the equation $k_2 - \frac{k_1^2}{4} = 0$.

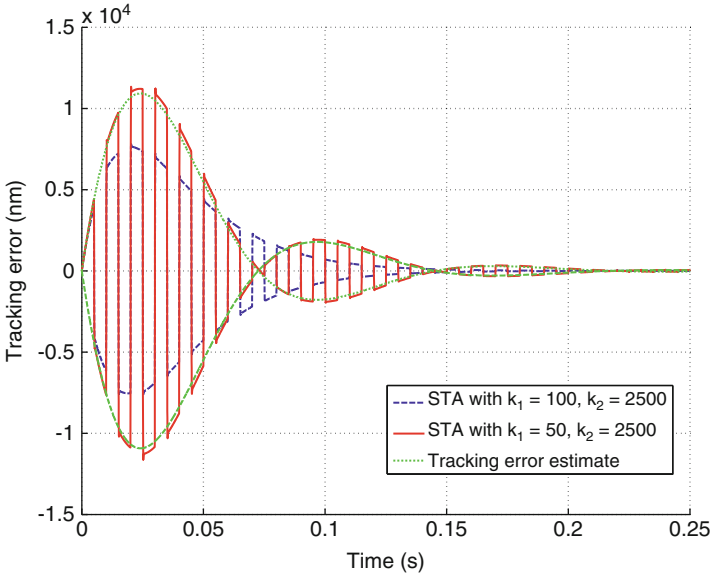

Fig. 5.9 The transient tracking error of STA as a function of the feedback controller gains. By choosing the controller gains carefully, a critically damped transient response can be achieved (*dashed blue line*). Oscillations may occur, however, for certain combinations of controller gains (*bold red line*). The transient tracking error can be quantified accurately (*dotted green line*). Figure ©Elsevier 2012, reprinted from [11] with permission

In the following example, the effect of k_1 and k_2 on the transient tracking error of STA is demonstrated. Assume that P is a second-order positioner with natural frequency 3,000 Hz and damping coefficient 0.8, and the reference signal is a triangular waveform of 100 Hz frequency and 5 µm amplitude. We will compare the tracking performance of the STA control architecture of Fig. 5.8a if two different feedback controllers are used. In the first controller, the integral gain coefficients are $k_1 = 100$ and $k_2 = 2,500$, so that $k_2 - \frac{k_1^2}{4} = 0$. In the second controller, $k_1 = 50$ and $k_2 = 2,500$. Figure 5.9 shows the tracking error for the first and second controller as dashed blue and solid red lines, respectively. As predicted by theory, the first controller exhibits a transient tracking error that converges exponentially to zero without oscillations. The tracking error of the second configuration also decays exponentially to zero, but, with undesirable transient oscillations. For the second configuration, the estimate of the transient tracking error based on (5.29) is shown as dashed green line. Equation (5.29) captures the tracking error exactly if $P(s) = 1$; for plants that are well damped and sufficiently fast, such as the one used in the simulation, (5.29) can be used as an accurate estimate of the tracking error.

The transient response of STA can be improved in several ways. In the most straightforward approach, STA can be simplified by removing the parasitic disturbance signal $g'(t)$ completely: as the preceding analysis shows, STA can be

implemented by merely inverting the signs of the input and the output of the feedback controller and using a constant feedforward term. Also, an equivalent performance can be achieved with the ISM-based control scheme of Fig. 5.8c. Other ways to improve the performance of STA are discussed in [11].

5.6 Experiments

In this section, the concept of impulsive control and its properties are demonstrated in an experimental setup. The experimental results are obtained on a custom-built AFM, a type of a scanning probe microscope.

A schematic of a common AFM setup is shown in Fig. 5.10. The sample under investigation is mounted on a nanopositioner, or scanner, which can move the sample in three degrees of freedom. To enable high-speed, high-resolution motion in the presence of external disturbances and modeling uncertainties, the scanner is typically equipped with highly sensitive noncontact sensors and operated in a feedback loop. During operation, the sample is brought into contact with the tip of a microfabricated cantilever and positioned relative to the tip along a two-dimensional scan trajectory, e.g., along a raster-based, spiral or Lissajous pattern. Properties of the sample, such as its topographical, electrical, or magnetic properties, are inferred from the nanoscale forces acting on the cantilever tip as the tip is moved across

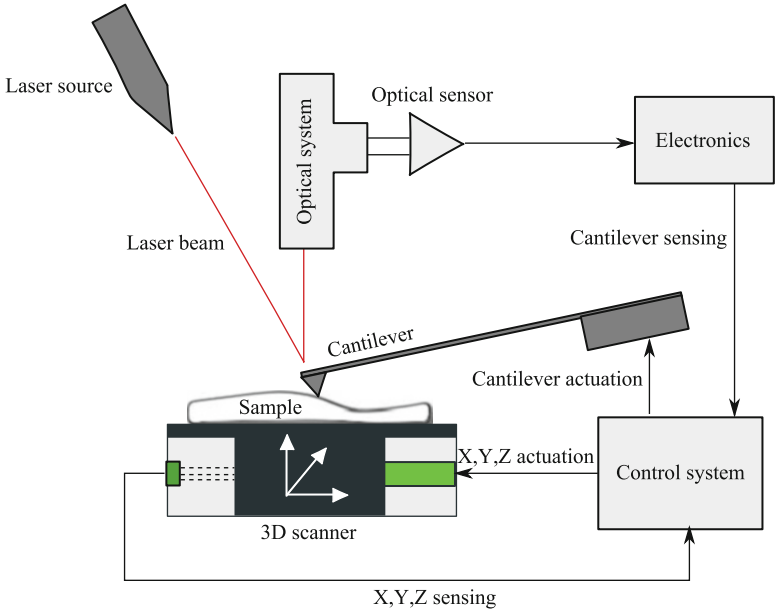

Fig. 5.10 Schematic of an atomic force microscope

the sample. In the schematic shown in Fig. 5.10, the deflection of the cantilever is estimated by means of an optical read-out system in which a laser beam is reflected from the cantilever tip, passes through an optical system and detected by means of a special-purpose optical sensor. The deflection of the cantilever provides an accurate estimate of the topography of the sample.

The feedback loop which controls the scanner motion is of key importance for the accuracy and speed of the AFM instrument. In the experiments described below, the feedback loop is equipped with an ISM-based hybrid controller or a linear feedback controller for comparison and used for high-speed AFM imaging. In the imaging experiments, a raster-based scan trajectory is followed by actuating the scanner in two orthogonal directions. In the fast, x-direction, a triangular reference signal is applied to scan the sample in consecutive scan lines; in the slow, y-direction, the position of the scanner is increased in discrete steps at the end of every scan line. In the x-scan direction, the nanopositioner uses a voice-coil actuator which is particularly suitable for this task because of its clean dynamics and linearity. In the y- and z-scan directions, a piezo-electric actuator is used. In the imaging experiments, thermomechanical cantilevers were used [50, 51]. The sample consists of nanolitograpically patterned nanostructures on silicon surface.

For the stability and performance of impulsive control and STA, the flat frequency response of the nanopositioner is of key importance. To that end, the mechanical resonances of the nanopositioner were damped by inverting its dynamics. The resulting transfer function could be approximated as $P(s) \approx 1$ in the frequency region below approx. 250 Hz. Owing to the voice-coil actuation principle, the dynamics of the scanner are highly linear, which is important for impulsive control. For positioners with significant nonlinearities, such as piezo-actuated positioners, additional compensation techniques might have to be employed, such as feedforward inversion [27] and charge amplifiers [46]. A magnetoresistive sensor [52] with a bandwidth exceeding 10 kHz was used to sense the position of the nanopositioner.

5.6.1 Impulsive Control for Tracking Piecewise Affine Signals

In this experiment, the performance of a linear feedback loop with and without ISM is compared and its effect on the quality of AFM imaging is demonstrated.

The control architecture used was the one shown in Fig. 5.3, with P denoting the shaped positioner dynamics along the fast scan axis. The feedback controller, K_{FB} was chosen as a simple integral controller such that the closed loop system had a very low bandwidth below 1 Hz. A benefit of such a scheme is that it minimizes the impact of measurement noise. The feedforward term K_{FF} was unity as the DC gain of the shaped positioner is 1.

The imaging was performed over an area of $3.5\,\mu\mathrm{m} \times 1.5\,\mu\mathrm{m}$ in a raster pattern. In the first case, the controller was only the linear feedback system as described above. In the second case, the linear feedback system was equipped with an ISM-based

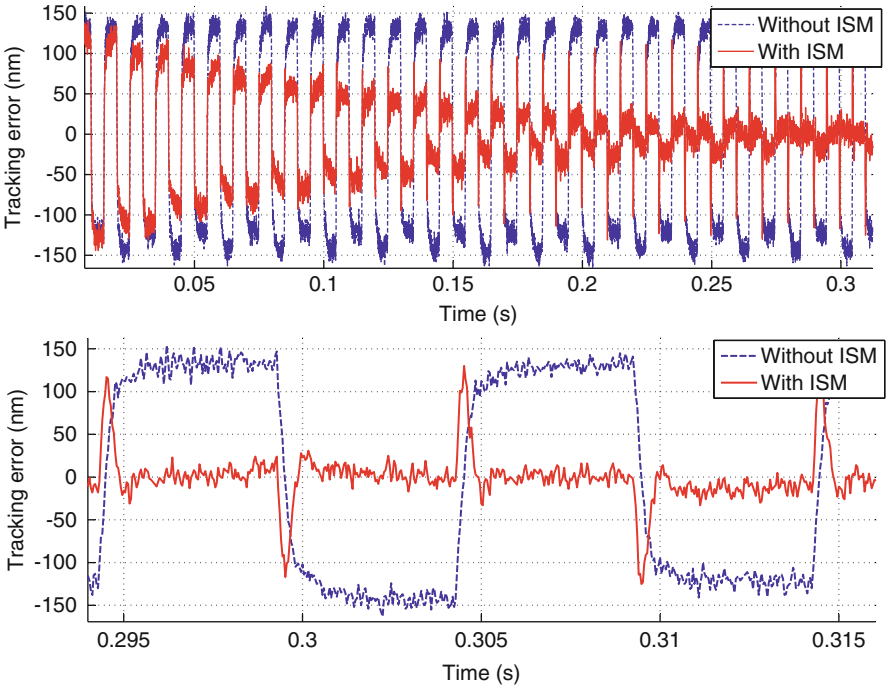

Fig. 5.11 Comparison of tracking error for closed loop without and with ISM. The *upper panel* shows the settling period of ISM, the *lower panel* shows the steady-state performance. The frequency of the reference signal was 100 Hz. Figure ©IOP Publishing 2011, reprinted from [10] with permission

impulsive control law as described in Sect. 5.4.2. Because the reference signal is a constant-amplitude, constant-frequency triangular waveform, the ISM control law simply inverted the sign of the accumulator of K at every turnaround point of r.

The tracking performance of the closed loop system with and without ISM is compared in Fig. 5.11. Using the ISM-based feedback controller, after a short settling time (top panel) near-zero steady-state error (bottom panel) was achieved; the convergence time corresponds to the rise time of the feedback loop $K/(1+K)$ under a step input which is consistent with the estimates presented in Sect. 5.5. The reduction of the positioning error is truly remarkable as it is enabled by the impulsive control law; the bandwidth of the linear control remains very low. This has a significant effect on the noise sensitivity of the control loop, an important aspect in nanopositioning as we shall see in the next section.

Figure 5.12 demonstrates how the tracking performance affects AFM imaging by comparing the images obtained using open loop control (on the left), feedback control without ISM (in the middle), and feedback control with ISM (on the right). The closed-loop image without ISM is similar to the open-loop image because of the very low bandwidth of the controller. The tracking lag resulted in an uncorrected,

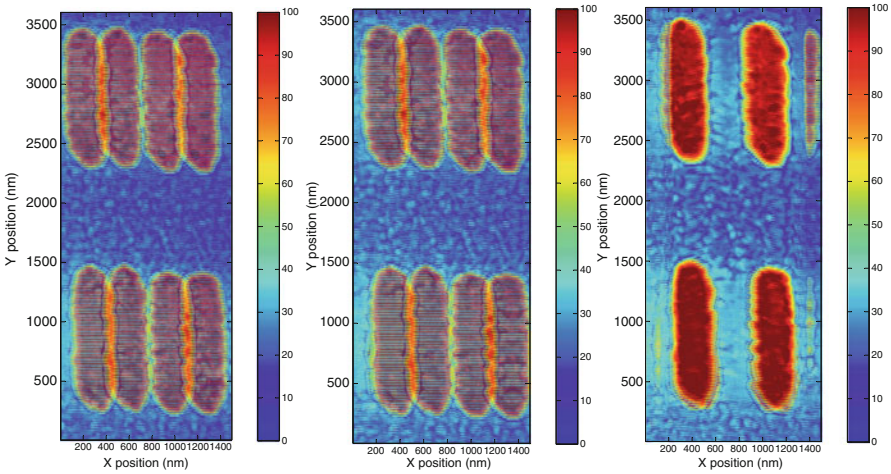

Fig. 5.12 The images of nanopatterns obtained with three different control schemes. The image on the *left* was acquired in open loop, using only the shaping of the positioner dynamics. The image in the *middle* was obtained using feedback control without ISM. The image on the *right* was acquired using feedback control with ISM. The height is in nanometers. The images were obtained in approx. 2 s. Figure ©IOP Publishing 2011, reprinted from [10] with permission

unknown shift in the image which was different for forward and backward scans. On the other hand, ISM removed the tracking lag almost perfectly without increasing the bandwidth of K. This not only resulted in detecting the real positions of the nanopatterns but also yielded consistent data in both scan directions, speeding up the imaging by a factor of two.

5.6.2 Sensitivity to Measurement Noise

In high-speed nanopositioning, measurement noise can significantly deteriorate the positioning accuracy. For example, in the control architecture of Fig. 5.3, additive measurement noise affects the measurement signal, enters the feedback loop, and is projected into the motion of the nanopositioner. An estimate of the nanopositioner motion induced by the measurement noise is an important figure in assessing the feedback control scheme and its suitability for nanopositioning. In the following, the nanopositioner motion induced by measurement noise is estimated for a high-bandwidth linear controller and an ISM-based controller of equivalent tracking performance.

The character and frequency spectrum of the measurement noise are determined by the position sensor. In what follows, a relatively noisy magnetoresistive position sensor is used to demonstrate the effect of ISM. The spectral characteristics of the measurement noise are presented in Fig. 5.13 and are largely dominated by *1/f* noise

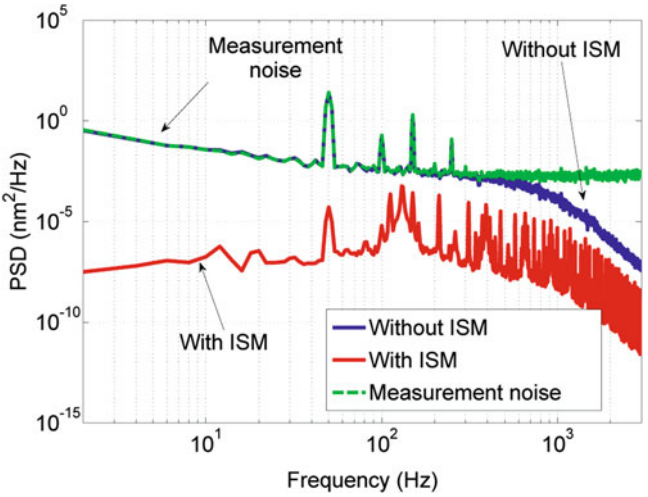

Fig. 5.13 Frequency spectra of the positioner motion induced by measurement noise. The measurement noise (*dashed green curve*) significantly affects the positioner motion if a high-bandwidth linear controller is used (*solid blue curve*). By using impulsive control, the positioning error introduced is significantly smaller (*red curve*) without compromising the tracking performance. Figure ©IEEE 2012, reprinted from [9] with permission

as is common for this type of sensor; spurious peaks occur at frequencies which are multiples of 50 Hz and are due to the ambient electrical noise. The standard deviation is approx. 9 nm over the frequency range from 0 Hz to 3 kHz.

For the purposes of a fair comparison, the ISM-based controller used in Sect. 5.6.1 was compared with a linear high gain integrator $K_{\mathrm{FB}}(s) = 1{,}530/s$. By increasing the gain of the integrator, the steady-state performance of both control schemes was made equivalent. The ISM-based and the linear controller were used to track a reference signal of frequency 130 Hz.

For the linear controller, the simulated spectral characteristics of the estimated positioning error are shown in Fig. 5.13 in blue. Because of the high bandwidth of the controller, the measurement noise at low frequencies significantly affects the motion of the positioner and induces a positioning error with a standard deviation of more than 8 nm over the frequency range examined.

For the ISM-based control scheme, the standard deviation of the positioning error is less than 1 nm over the frequency range from 0 Hz to 3 kHz. The spectral characteristics are shown in Fig. 5.13 in red. This improvement in resolution is achieved even though the tracking performance is not compromised; in fact, the transient tracking performance of the ISM-based controller is even better than that of the linear controller. However, there are additional peaks in the frequency spectrum which are induced by the impulsive changes of the controller state. In particular, the spectral component at 130 Hz corresponds to the frequency of the signal tracked. Further spectral components at frequencies which are multiples

of 130 Hz occur because of the discontinuous evolution of the state. However, these spectral components have only minimal influence on the overall tracking performance. Moreover, they are not strongly affected by the closed-loop dynamics because the impulsive control law is of feedforward type and is fully determined by the reference signal.

5.6.3 *Multiobjective Impulsive Control: Tracking and Disturbance Rejection*

Impulsive control can be applied to feedback controllers with a complex structure, such as those designed for achieving multiple control objectives simultaneously. To demonstrate this, a feedback controller for the control architecture of Fig. 5.3 is presented which can track a fast triangular waveform in the presence of a sinusoidal input disturbance.

The feedback controller consists of a tracking component, a disturbance rejection component and an ISM-based component. Using the notation introduced in Sect. 5.4.3, the controller takes the form

$$K_{\mathrm{FB}}(s) = K_{\mathrm{FB}}^{R}(s) + K_{\mathrm{FB}}^{Di}(s), \tag{5.30}$$

where $K_{\mathrm{FB}}^{R}(s) = k/s$ is the tracking component, here a single integrator with gain k, and K_{FB}^{Di} rejects the sinusoidal input disturbance. For example, K_{FB}^{Di} can be a peak filter or a model-based controller. To track the fast triangular waveform with low gain k, K_{FB}^{R} is extended with an impulsive control law as in the previous experiments. On the other hand, given the type of the disturbance, the states of K_{FB}^{Di} are not affected by the impulsive control law and evolve linearly.

This feedback controller was used for high-speed AFM imaging in the presence of significant input disturbance that would cause scanner motion of more than 500 nm in the absence of control. Figure 5.14 compares the images taken in open-loop mode and with the feedback controller. In open-loop mode, the image is heavily distorted by the input disturbance, as is evident in Fig. 5.14a. By using the proposed controller, the effect of the input disturbance is minimized and at the same time, excellent tracking performance is achieved (Fig. 5.14b).

5.6.4 *Transient Performance of STA and Impulsive Control*

Section 5.5 provided a detailed analysis of the relation between impulsive control and the recently published STA. It was shown that for triangular waveform tracking, both schemes are inherently linked and essentially equivalent. Importantly, one of the conclusions in the theoretical analysis was that impulsive control has

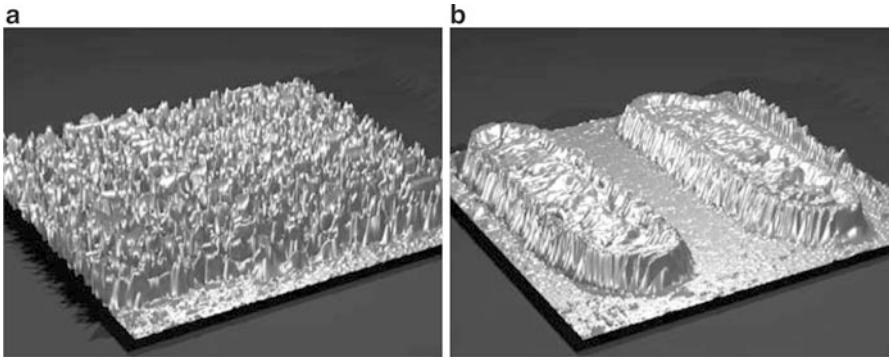

Fig. 5.14 High-speed AFM images of approx. $1,000 \times 250 \times 100$ nm titanium nitride nanopatterns taken in the presence of a significant input disturbance. The image in (**a**) was acquired in open-loop; the image in (**b**) was acquired using a feedback controller with combined control objectives for tracking and disturbance rejection. It demonstrates the combination of impulsive and linear control: the good tracking performance was obtained with only a low-gain integrator with ISM. Moreover, at the same time, the effect of the input disturbance was minimized. Figure ©IEEE 2012, reprinted from [9] with permission

significantly less transient tracking error than STA while having the same steady-state performance. In the following, experiments are presented which compare impulsive control with STA.

The STA control architecture was implemented as shown in Fig. 5.8a. A double integral controller

$$K(s) = \frac{50}{s} + \frac{1,000}{s^2} \tag{5.31}$$

was used together with the pair of signal transformation operators Φ, Φ^{-1} as defined in Sect. 5.5.1. By doing so, the triangular reference signal was transformed into a ramp signal which was tracked by the feedback controller K.

In the control architecture based on impulsive control, the control scheme of Fig. 5.3 was used with the feedforward term $K_{\mathrm{FF}}(s) = 1$ and the feedback controller

$$K_{\mathrm{FB}}(s) = \frac{50}{s} \tag{5.32}$$

As the DC gain of the positioner was known exactly, a single integrator was sufficient to provide a near-zero tracking error in the steady state. The state of the feedback controller was multiplied by -1 at every turnaround point of the triangular reference signal. The factor of -1 is the ratio of the successive slopes of the single frequency triangular signal.

Figure 5.15 compares the tracking performance of STA and impulsive control. As predicted by theory, the transient phase of STA is dominated by a large overshoot which exponentially decays to zero. Because of the overshoot, the amplitude of the reference signal had to be limited so that the scanner stroke was not exceeded

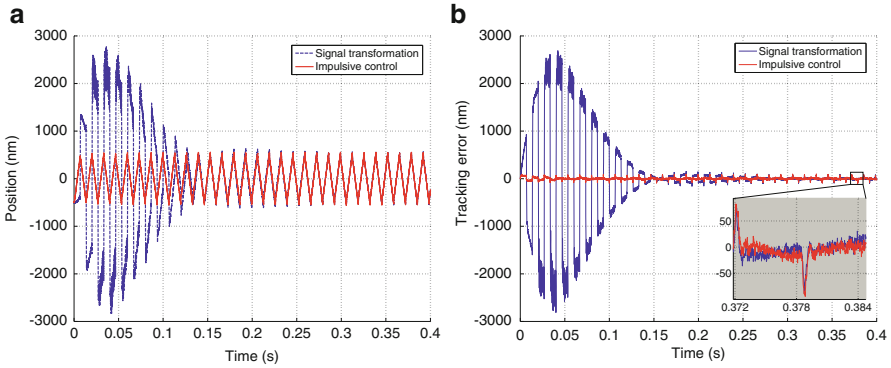

Fig. 5.15 Tracking of a fixed frequency triangular waveform with a control architecture based on impulsive control in *blue* and signal transformation approach in *red*. The frequency of the reference signal was 75 Hz and the amplitude was 1 µm. (**a**) Tracking output (position). (**b**) Tracking error. Figure ©Elsevier 2012, reprinted from [11] with permission

in the transient phase. The transient effects also induced unwanted mechanical vibrations. The transient phase of the impulsive control scheme did not suffer from the overshoot present in STA and quickly achieved the convergence as discussed in Sect. 5.5.4. The steady state performance of both schemes was comparable.

5.7 Conclusion

We have reviewed a novel hybrid control approach to nanopositioning that is based on the concept of impulsive control. In impulsive control, the states of a feedback controller are changed abruptly at discrete instances in time. We have analyzed the stability of impulsive control systems and introduced feedback control architectures based on impulsive control, including control architectures for tracking piecewise constant and piecewise affine signals and multiobjective hybrid feedback control. We discussed the inherent connection between impulsive control and the recently published STA to nanopositioning. The theoretical findings are supported by experiments in which impulsive control was used in a high-speed AFM. The experiments show that by using impulsive control, the tracking error in AFM can be minimized without increasing the bandwidth of the linear controller, thereby speeding up the AFM imaging process by a factor of two without increasing the sensitivity of the feedback loop to measurement noise. We have also demonstrated impulsive feedback control in the presence of a significant input disturbance and experimentally compared the performance of impulsive control and the signal transformation approach. The theoretical and experimental results indicate that impulsive control for nanopositioning has a significant potential for practical applications and at the same time fosters new research directions in the theoretical understanding of hybrid feedback control.

Acknowledgements We thank Urs Egger and Walter Häberle for their support with the mechanical and electronic hardware used in the experiments. Special thanks go to Haris Pozidis and Evangelos Eleftheriou for their support of this work.

References

1. G. Binnig, H. Rohrer, C. Gerber, E. Weibel, Surface studies by scanning tunneling microscopy. Phys. Rev. Lett. **49**(1), 57–61 (1982)
2. G. Binnig, C. Quate, C. Gerber, Atomic force microscope. Phys. Rev. Lett. **56**(9), 930–933 (1986)
3. L. Gross, F. Mohn, N. Moll, B. Schuler, A. Criado, E. Guitián, D. Peña, A. Gourdon, G. Meyer, Bond-order discrimination by atomic force microscopy. Science **337**(6100), 1326–1329 (2012)
4. D. Pires, J.L. Hedrick, A.D. Silva, J. Frommer, B. Gotsmann, H. Wolf, M. Despont, U. Duerig, A.W. Knoll, Nanoscale three-dimensional patterning of molecular resists by scanning probes. Science **328**, 732–735 (2010)
5. T. Ando, High-speed atomic force microscopy coming of age. Nanotechnology **23**, 062001 (2012)
6. E. Eleftheriou, T. Antonakopoulos, G. Binnig, G. Cherubini, M. Despont, A. Dholakia, U. Durig, M. Lantz, H. Pozidis, H. Rothuizen, P. Vettiger, Millipede - a MEMS-based scanning-probe data-storage system. IEEE Trans. Magn. **39**(2) 938–945 (2003)
7. A. Pantazi, A. Sebastian, T.A. Antonakopoulos, P. Baechtold, A.R. Bonaccio, J. Bonan, G. Cherubini, M. Despont, R.A. DiPietro, U. Drechsler, U. Duerig, B. Gotsmann, W. Haeberle, C. Hagleitner, J.L. Hedrick, D. Jubin, A. Knoll, M.A. Lantz, J. Pentarakis, H. Pozidis, R.C. Pratt, H. Rothuizen, R. Stutz, M. Varsamou, D. Wiesmann, E. Eleftheriou, Probe-based ultrahigh-density storage technology. IBM J. Res. Develop. **52**(4.5), 493–511 (2008)
8. R.A. Oliver, Advances in AFM for the electrical characterization of semiconductors. Rep. Progr. Phys. **71**(7), 076501 (2008)
9. T. Tuma, A. Pantazi, J. Lygeros, A. Sebastian, Nanopositioning with impulsive state multiplication: a hybrid control approach. IEEE Trans. Contr. Syst. Technol. (2012, to appear)
10. T. Tuma, A. Sebastian, W. Häberle, J. Lygeros, A. Pantazi, Impulsive control for fast nanopositioning. Nanotechnology **22**, 135501 (2011)
11. T. Tuma, A. Pantazi, J. Lygeros, A. Sebastian, Comparison of two non-linear control approaches to fast nanopositioning: impulsive control and signal transformation. Mechatronics **22**, 302–309 (2012)
12. T. Tuma, A. Pantazi, J. Lygeros, A. Sebastian, Impulsive control for nanopositioning: stability and performance, in *Proceedings of the 14th International Conference on Hybrid Systems: Computation and Control*, ACM, pp. 173–180 (2011)
13. S.M. Salapaka, M.V. Salapaka, Scanning probe microscopy. IEEE Contr. Syst. Mag. **28**(2), 65–83 (2008)
14. D. Abramovitch, S. Andersson, L. Pao, G. Schitter, A tutorial on the mechanisms, dynamics, and control of atomic force microscopes, in *Proceedings of the American Control Conference*, IEEE, pp. 3488–3502 (2007)
15. S. Devasia, E. Eleftheriou, S.O.R. Moheimani, A survey of control issues in nanopositioning. IEEE Trans. Contr. Syst. Technol. **15**(5), 802–823 (2007)
16. S. Aphale, A. Fleming, S. Reza Moheimani, Integral resonant control of collocated smart structures. Smart Mater. Struct. **16**, 439 (2007)
17. A. Fleming, S. Aphale, S. Moheimani, A new method for robust damping and tracking control of scanning probe microscope positioning stages. IEEE Trans. Nanotechnol. **9**(4), 438–448 (2010)

18. A. Sebastian, A. Pantazi, S.O.R. Moheimani, H. Pozidis, E. Eleftheriou, Achieving sub-nanometer precision in a MEMS-based storage device during self-servo write process. IEEE Trans. Nanotechnol. **7**(5), 586–595 (2008)
19. G. Schitter, R. Stark, A. Stemmer, Fast contact-mode atomic force microscopy on biological specimen by model-based control. Ultramicroscopy **100**(3), 253–257 (2004)
20. S. Salapaka, A. Sebastian, J.P. Cleveland, M.V. Salapaka, High bandwidth nano-positioner: a robust control approach. Rev. Sci. Instrum. **73**(9), 3232–3241 (2002)
21. A. Sebastian, S. Salapaka, Design methodologies for robust nano-positioning. IEEE Trans. Contr. Syst. Technol. **13**(6), 868–876 (2005)
22. C. Lee, S.M. Salapaka, Robust broadband nanopositioning: fundamental trade-offs, analysis, and design in a two-degree-of-freedom control framework. Nanotechnology **20**(3), 035501 (2009)
23. S. Bashash, N. Jalili, Robust adaptive control of coupled parallel piezo-flexural nanopositioning stages. IEEE/ASME Trans. Mechatron. **14**(1), 11–20 (2009)
24. S. Hara, Y. Yamamoto, T. Omata, M. Nakano, Repetitive control system: a new type servo system for periodic exogenous signals. IEEE Trans. Automat. Contr. **33**(7), 659–668 (1988)
25. Y. Shan, K. Leang, Repetitive control with Prandtl-Ishlinskii hysteresis inverse for piezo-based nanopositioning, in *Proceedings of the American Control Conference*, IEEE, pp. 301–306 (2009)
26. D. Bristow, M. Tharayil, A. Alleyne, A survey of iterative learning control. IEEE Contr. Syst. Mag. **26**(3), 96–114 (2006)
27. K. Leang, Q. Zou, S. Devasia, Feedforward control of piezoactuators in atomic force microscope systems. IEEE Contr. Syst. Mag. **29**, 70–82 (2009)
28. N.C. Singer, W.P. Seering, Preshaping command inputs to reduce system vibration. J. Dyn. Syst. Meas. Contr. **112**(1), 76–82 (1990)
29. A. Fleming, A. Wills, Optimal periodic trajectories for band-limited systems. IEEE Trans. Contr. Syst. Technol. **17**(3), 552–562 (2009)
30. I. Mahmood, S. Reza Moheimani, Fast spiral-scan atomic force microscopy. Nanotechnology **20**, 365503 (2009)
31. A. Kotsopoulos, T. Antonakopoulos, Nanopositioning using the spiral of archimedes: the probe-based storage case. Mechatronics **20**(2), 273–280 (2010)
32. A. Kotsopoulos, A. Pantazi, A. Sebastian, T. Antonakopoulos, High-speed spiral nanopositioning, in *Proceedings of IFAC world congress*, IFAC, pp. 2018–2023 (2011)
33. Y. Yong, S. Moheimani, I. Petersen, High-speed cycloid-scan atomic force microscopy. Nanotechnology **21**, 365503 (2010)
34. T. Tuma, J. Lygeros, V. Kartik, A. Sebastian, A. Pantazi, High-speed multiresolution scanning probe microscopy based on Lissajous scan trajectories. Nanotechnology **23**, 185501 (2012)
35. T. Tuma, J. Lygeros, A. Sebastian, A. Pantazi, Optimal scan trajectories for high speed scanning probe microscopy, in *Proceedings of the 2012 American Control Conference*, IEEE, pp. 3791–3796 (2012)
36. R. Goebel, R. Sanfelice, A. Teel, Hybrid dynamical systems. IEEE Contr. Syst. Mag. **29**(2), 28–93 (2009)
37. D. Liberzon, *Switching in Systems and Control*. Ser. Systems & Control: Foundations & Applications (Birkhäuser, Boston, 2003)
38. J.C. Clegg, A nonlinear integrator for servomechanisms. Trans. AIEE, Part II. Appl. Ind. **77**(2), 41–42 (1958)
39. I. Horowitz, P. Rosenbaum, Non-linear design for cost of feedback reduction in systems with large parameter uncertainty. Int. J. Contr. **21**, 977–1001 (1975)
40. D. Nesic, L. Zaccarian, A.R. Teel, Stability properties of reset systems. Automatica **44**, 2019–2026 (2008)
41. D. Wu, G. Guo, Y. Wang, Reset integral-derivative control for HDD servo systems. IEEE Trans. Contr. Syst. Technol. **15**(1), 161–167 (2007)

42. D.D. Bainov, P.S. Simeonov, *Systems with Impulse Effect: Stability, Theory and Applications*. Ser. Ellis Horwood Series: Mathematics and Its Applications. Chichester, UK (Ellis Horwood, 1989)
43. G. Schitter, K.J. Astrom, B.E. DeMartini, P.J. Thurner, K.L. Turner, P.K. Hansma, Design and modeling of a high-speed AFM-Scanner. IEEE Trans. Contr. Syst. Technol. **15**(5), 906–915 (2007)
44. S.O.R. Moheimani, B.J.G. Vautier, Resonant control of structural vibration using charge-driven piezoelectric actuators. IEEE Trans. Contr. Syst. Technol. **13**(6), 1021–1035 (2005)
45. A.J. Fleming, S.O.R. Moheimani, Sensorless vibration suppression and scan compensation for piezoelectric tube nanopositioners. IEEE Trans. Contr. Syst. Technol. **14**(1), 33–44 (2006)
46. A. Fleming, S. Moheimani, A grounded-load charge amplifier for reducing hysteresis in piezoelectric tube scanners. Rev. Sci. Instrum. **76**(7), 073707 (2005)
47. A. Sebastian, S.O.R. Moheimani, Signal transformation approach to fast nanopositioning. Rev. Sci. Instrum. **80**(7), 076101-1–076101-3 (2009)
48. A. Bazaei, S.O.R. Moheimani, A. Sebastian, An analysis of signal transformation approach to triangular waveform tracking. Automatica **47**(4), 838–847 (2011)
49. A. Bazaei, Y. Yong, S. Moheimani, A. Sebastian, Tracking of triangular references using signal transformation for control of a novel AFM scanner stage. IEEE Trans. Contr. Syst. Technol. **20**(2), 453–464 (2012)
50. H. Rothuizen, M. Despont, U. Drechsler, C. Hagleitner, A. Sebastian, D. Wiesmann, Design of power-optimized thermal cantilevers for scanning probe topography sensing, in *Proceedings of IEEE 22nd International Conference on Micro Electro Mechanical Systems*, IEEE, pp. 603–606 (2009)
51. A. Sebastian, D. Wiesmann, Modeling and experimental identification of silicon microheater dynamics: a systems approach. IEEE/ASME J. Microelectromech. Syst. **17**(4), 911–920 (2008)
52. V. Kartik, A. Sebastian, T. Tuma, A. Pantazi, H. Pozidis, D. Sahoo, High-bandwidth nanopositioner with magnetoresistance based position sensing. Mechatronics **22**, 295–301 (2012)